Cell Host & Microbe, Volume *29*

Supplemental information

Comprehensive mapping of mutations in the SARS-CoV-2 receptor-binding domain that affect recognition by polyclonal human plasma antibodies

Allison J. Greaney, Andrea N. Loes, Katharine H.D. Crawford, Tyler N. Starr, Keara D. Malone, Helen Y. Chu, and Jesse D. Bloom

Supplementary Table 2. Percentage of RBD mutant library that fell into FACS "escape gate" for each plasma during the mapping, related to Figure 2.

Plasma is a unique identifier for each plasma mapped, PID is the patient ID from (Crawford et al., 2020a), subject is the simpler patient identifier used for patients in the current study, the selection plasma dilution indicates the reciprocal dilution at which each selection was performed (i.e., 500 is a 1:500 dilution of plasma) and the 4 rightmost columns indicate the percentage of each population of cells that fell into the antibody-escape selection gate for the duplicate mutant libraries (lib1 and lib2) and for cells expressing unmutated RBD and incubated with the same dilution of plasma as the mutant libraries (WT 1x) or 10-fold less plasma (WT 0.1x).

There are no corresponding raw FACSDiva gating plots for expt_36 (subject K (day 29)) in **Figure S2**.

						percentage of RBD+ cells in escape gate			
experiment	**plasma**	**PID**	**subject**	**days post-symptom onset**	**selection plasma dilution**	**lib1**	**lib2**	**WT 1x**	**WT 0.1x**
expt_34	23_d21	23	A	21	1250	2.6	1.7	0.2	3.2
expt_39	23_d45	23	A	45	1250	3.1	2.5	0.1	10.8
expt_50	23_d120	23	A	120	500	4.5	6.4	0.1	27.5
expt_41	1C_d26	1C	B	26	200	4.5	3.6	0.1	0.3
expt_51	1C_d113	1C	B	113	200	3.7	4.7	0	0.4
expt_35	24C_d32	24C	C	32	200	6.7	6.5	0	0.2
expt_44	24C_d104	24C	C	104	200	4.6	5.5	1	1.9
expt_30	6C_d33	6C	D	33	500	5.1	4.7	0.1	27.4
expt_42	6C_d76	6C	D	76	500	4.3	3.8	0.1	1.2
expt_38	22C_d28	22C	E	28	200	4.7	2.9	0	0.9
expt_45	22C_d104	22C	E	104	200	5	4.4	1.8	1.7
expt_48	25C_d48	25C	F	48	200	4	5	0.2	37.7
expt_49	25C_d115	25C	F	115	80	4.4	5.9	0.2	30.8
expt_32	25_d18	25	G	18	500	5.1	5.9	0.1	3.5
expt_33	25_d94	25	G	94	200	5.2	4.2	0.3	44.8
expt_37	12C_d61	12C	H	61	160	3.3	3.1	0	0.3
expt_40	12C_d152	12C	H	152	80	4	5.2	0	0.7
expt_46	23C_d26	23C	I	26	80	2.7	4.6	0	1.8
expt_47	23C_d102	23C	I	102	80	3	5.8	0	0.5
expt_31	13_d15	13	J	15	200	4.4	5.7	0.1	71.3
expt_52	13_d121	13	J	121	1250	4.2	4.8	0.1	7.2
expt_36	7C_d29	7C	K	29	500	6.1	6.1	0	0.7
expt_43	7C_d103	7C	K	103	200	4.9	4.9	0.5	15.5

A

Subject	Sex	Age (y)	Severity
subject A	Male	56	Hospitalized
subject B	Male	35	Hospitalized
subject C	Female	76	Non-Hospitalized
subject D	Female	64	Hospitalized
subject E	Male	65	Non-Hospitalized
subject F	Female	52	Non-Hospitalized
subject G	Female	31	Hospitalized
subject H	Male	68	Non-Hospitalized
subject I	Female	65	Non-Hospitalized
subject J	Male	54	Hospitalized
subject K	Male	65	Non-Hospitalized
subject L	Female	68	Asymptomatic
subject M	Male	56	Non-Hospitalized
subject N	Male	23	Non-Hospitalized
subject P	Male	29	Non-Hospitalized
subject Q	Female	47	Non-Hospitalized
subject R	Female	24	Asymptomatic

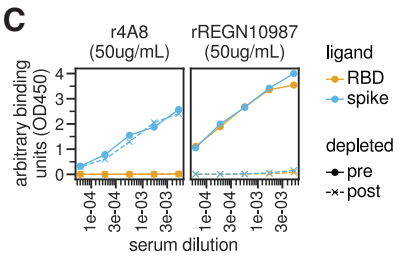

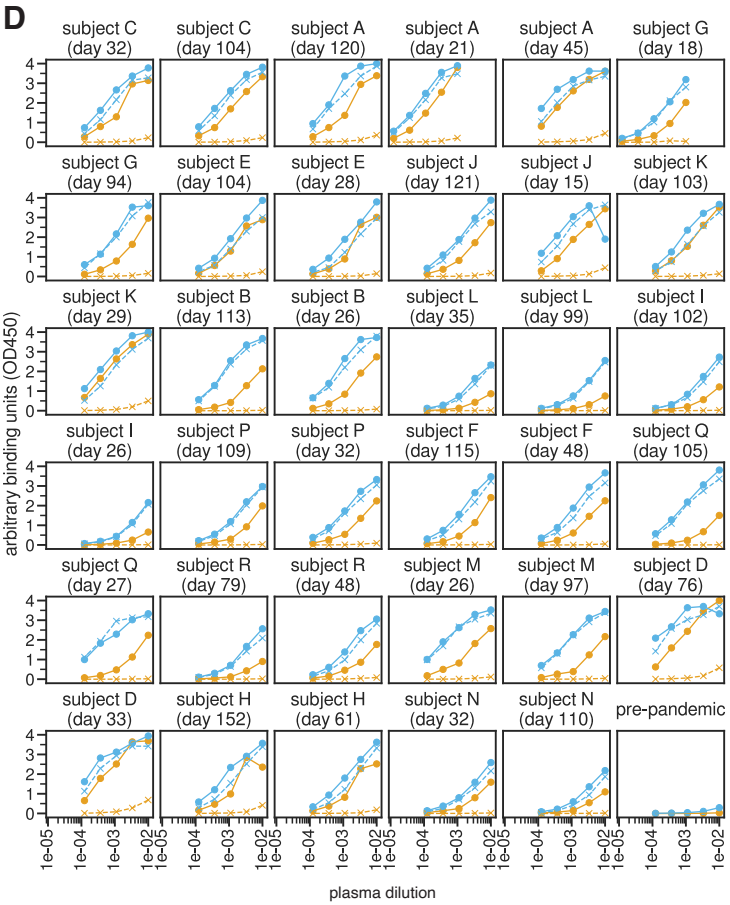

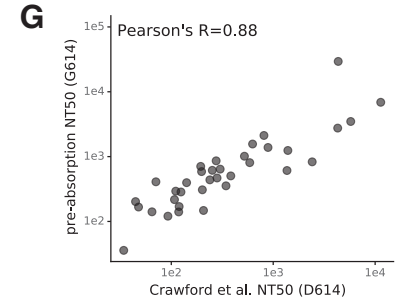

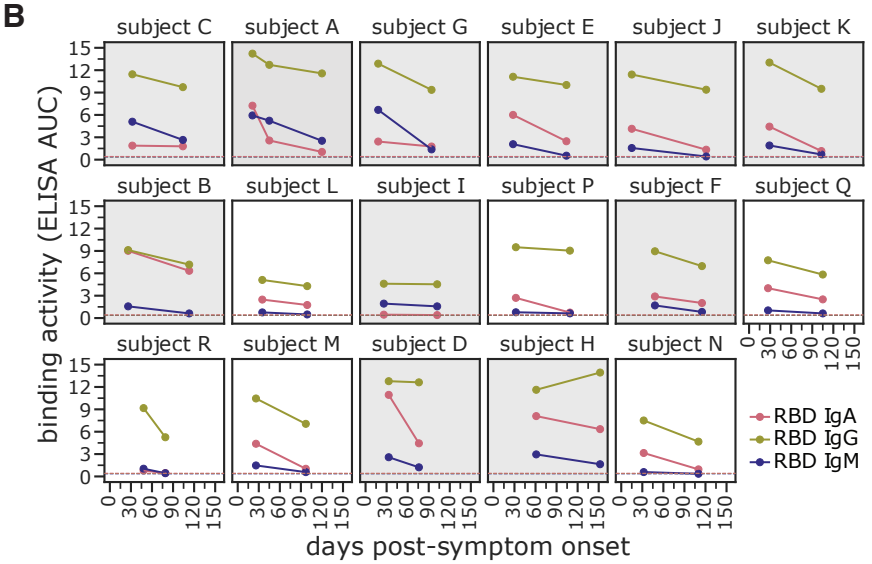

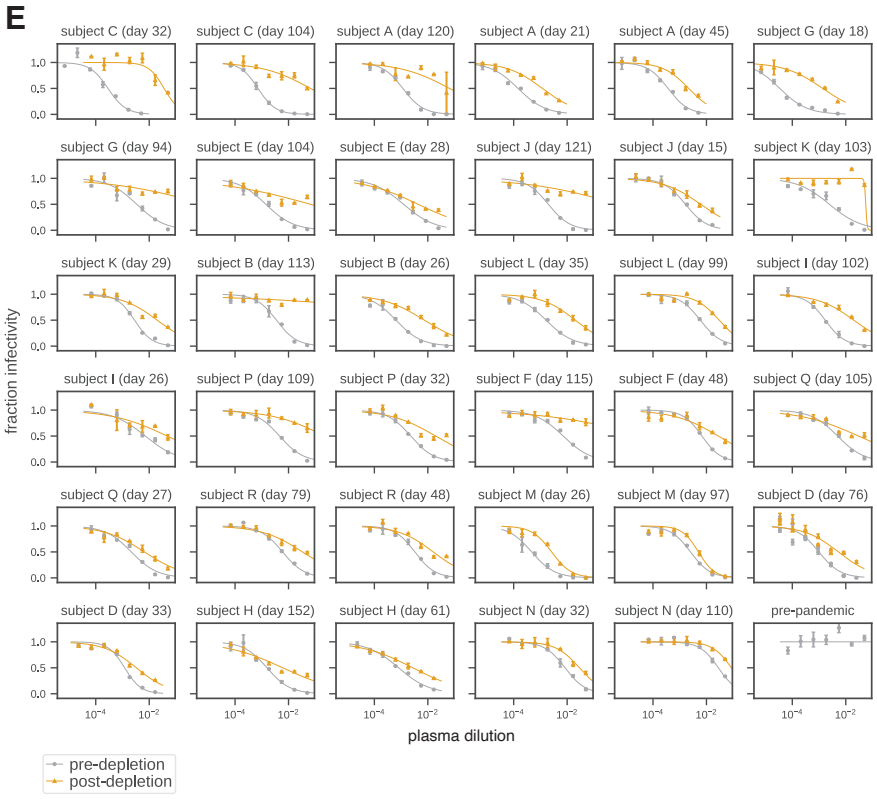

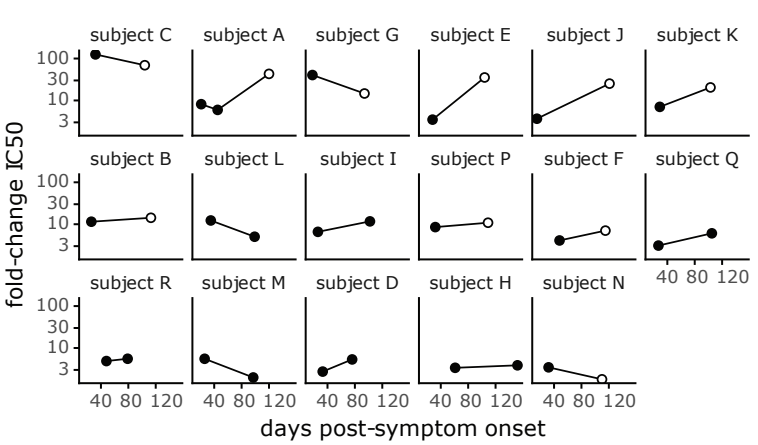

Figure S1. **Raw ELISA and neutralization curves of plasma pre- and post-depletion of RBD-targeting antibodies, related to Figure 1. (A)** Participant sex, age (y), and disease severity. **(B)** Previously measured RBD binding for three antibody isotypes for these plasma samples as measured by ELISA area under the curve (AUC), taken from (Crawford et al., 2020a). Gray background indicates plasma for which we subsequently mapped mutations that reduce binding. Similar data across additional time points not used in the current study are available in (Crawford et al., 2020a); see **Supplementary Table 1** to map between the sample IDs used in the current study and (Crawford et al., 2020a). **(C)** Effect of RBD antibody depletion on binding to RBD and spike by "synthetic sera" comprised of pre-pandemic pooled plasma with the NTD-targeting antibody r4A8 (Chi et al., 2020) or RBD-targeting antibody rREGN10987 (Hansen et al., 2020). Antibodies were added to pre-pandemic plasma at 50 µg/mL. The x-axis indicates the dilution factor of the plasma+antibody mix, and the y-axis is the ELISA reading at each dilution. **(D)** Raw ELISA binding curves of plasma to RBD and spike before and after depletion of RBD-binding antibodies. Legend for panels **(C)** and **(D)**: orange is RBD binding, blue is spike binding; filled circles with solid lines represent pre-depletion, and x's with dashed lines represent post-depletion of anti-RBD antibodies. **(E)** Raw neutralization curves for plasma before (gray) and after (orange) depletion of RBD-binding antibodies. Neutralization assays were performed with lentiviruses pseudotyped with spike D614G, the predominant SARS-CoV-2 circulating variant. **(F)** Change in the amount of neutralizing activity that is due to RBD-binding antibodies over time for each individual. Each point gives the fold-change in neutralization inhibitory concentration 50% (IC50) post- versus pre-depletion for plasma isolated at the indicated time, such that larger values indicate that more of the neutralizing activity is due to RBD-binding antibodies. Open circles represent samples for which the post-depletion NT50 was at the limit of detection, i.e., less than 20 (see **Figure 1B**); these circles are therefore lower bounds in the fold-change in IC50. **(G)** Correlation between previously measured neutralization titers 50% (NT50) with spike D614-spike-pseudotyped lentivirus (Crawford et al., 2020a) and pre-depletion neutralization titers measured with G614-spike-pseudotyped lentivirus (present study), Pearson's R = 0.88.

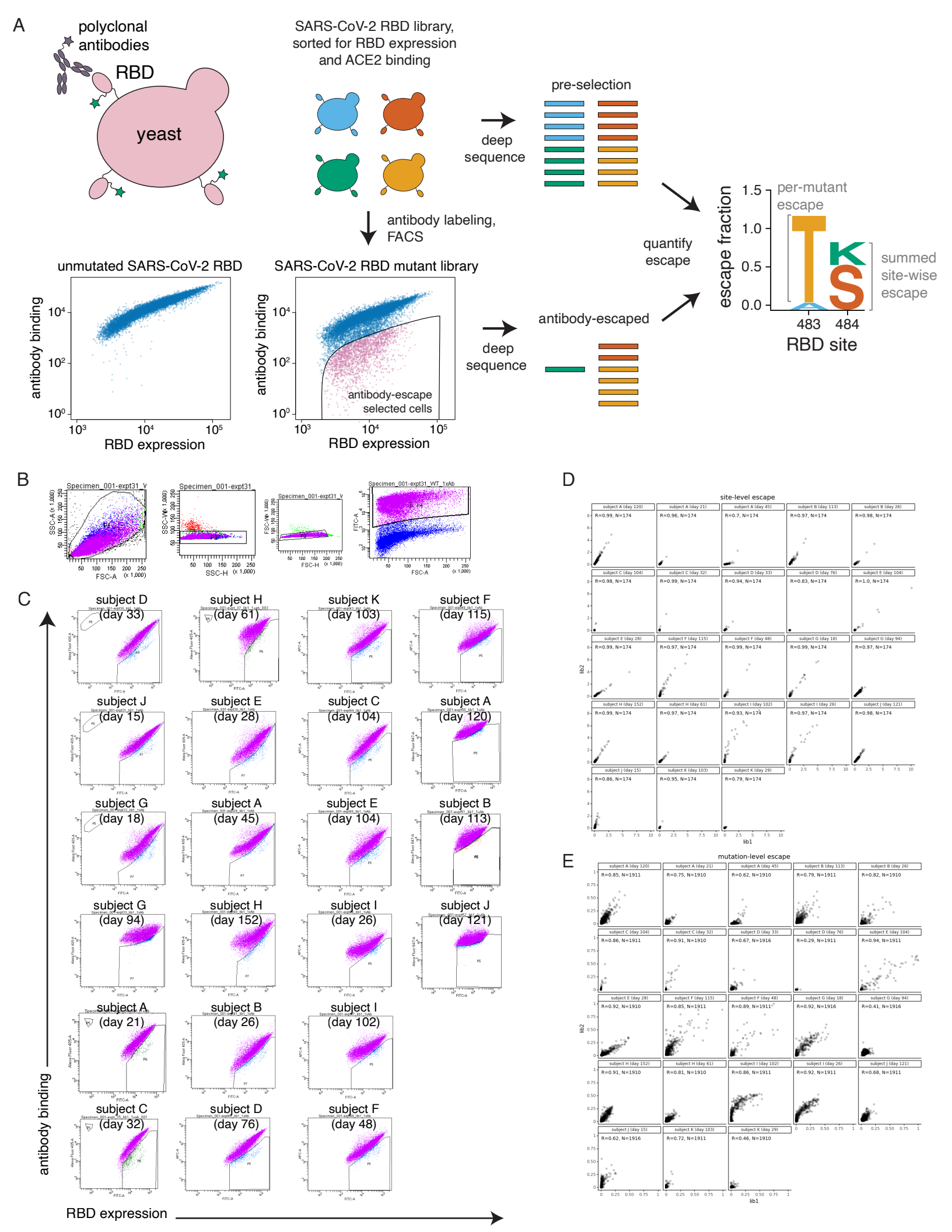
A
polyclonal antibodies
RBD
yeast
SARS-CoV-2 RBD library, sorted for RBD expression and ACE2 binding
deep sequence
pre-selection
antibody labeling, FACS
unmutated SARS-CoV-2 RBD
SARS-CoV-2 RBD mutant library
antibody binding
RBD expression
antibody-escape selected cells
deep sequence
antibody-escaped
quantify escape
escape fraction
per-mutant escape
summed site-wise escape
RBD site
B
C
subject D (day 33)
subject H (day 61)
subject K (day 103)
subject F (day 115)
subject J (day 15)
subject E (day 28)
subject C (day 104)
subject A (day 120)
subject G (day 18)
subject A (day 45)
subject E (day 104)
subject B (day 113)
subject G (day 94)
subject H (day 152)
subject I (day 26)
subject J (day 121)
subject A (day 21)
subject B (day 26)
subject I (day 102)
subject C (day 32)
subject D (day 76)
subject F (day 48)
antibody binding
RBD expression
D
site-level escape
E
mutation-level escape

Figure S2. **Approach for mapping RBD mutations that reduce binding by polyclonal plasma, related to Figure 2. (A)** The RBD is expressed on the surface of yeast. Flow cytometry can be used to quantify both RBD expression (via a C-terminal MYC tag) and antibody binding to the RBD protein expressed on the surface of each yeast cell. A library of yeast expressing different RBD mutants were incubated with polyclonal plasma and plasma antibody binding was detected using a IgA+IgG+IgM secondary antibody. We then used FACS to enrich for cells expressing RBD that bound reduced levels of antibody, and used deep sequencing to quantify the frequency of each mutation in the initial and "antibody escape" cell populations. We quantified the effect of each mutation as the "escape fraction," which represents the fraction of cells expressing RBD with that mutation that fell in the "antibody escape" FACS bin. Escape fractions are represented in logo plots, with the height of each letter proportional to the effect of that amino acid mutation on antibody binding. The site-level escape metric is the sum of the escape fractions of all mutations at a site. Note that both experimental and computational filtering steps were used to remove RBD mutants that were misfolded or completely unable to bind the ACE2 receptor (see **Methods**). **(B)** Representative plots of nested FACS gating strategy used for all plasma selection experiments to select for single cells (SSC-A vs. FSC-A, and FSC-W vs. FSC-H) that also express RBD (FITC-A vs. FSC-A). **(C)** FACS gating strategy for one of two independent libraries to select cells expressing RBD mutants with reduced binding by polyclonal plasma. Gates were set manually during sorting, aiming for 3-6% of the RBD+ library to fall into the selection gate (cells in blue). The same gate was set for both independent libraries stained with each plasma, and the FACS scatter plots looked qualitatively similar between the two libraries. For information on the fraction of library cells that fall into each selection gate, see **Supplementary Table 2**. **(D)** Correlation plots of site-level escape for each of the two independent RBD mutant libraries for each plasma. Site-level escape is the sum of escape fraction for each mutation at a site. **(E)** Correlation plots of mutation-level escape for each of the two independent RBD mutant libraries for each plasma.

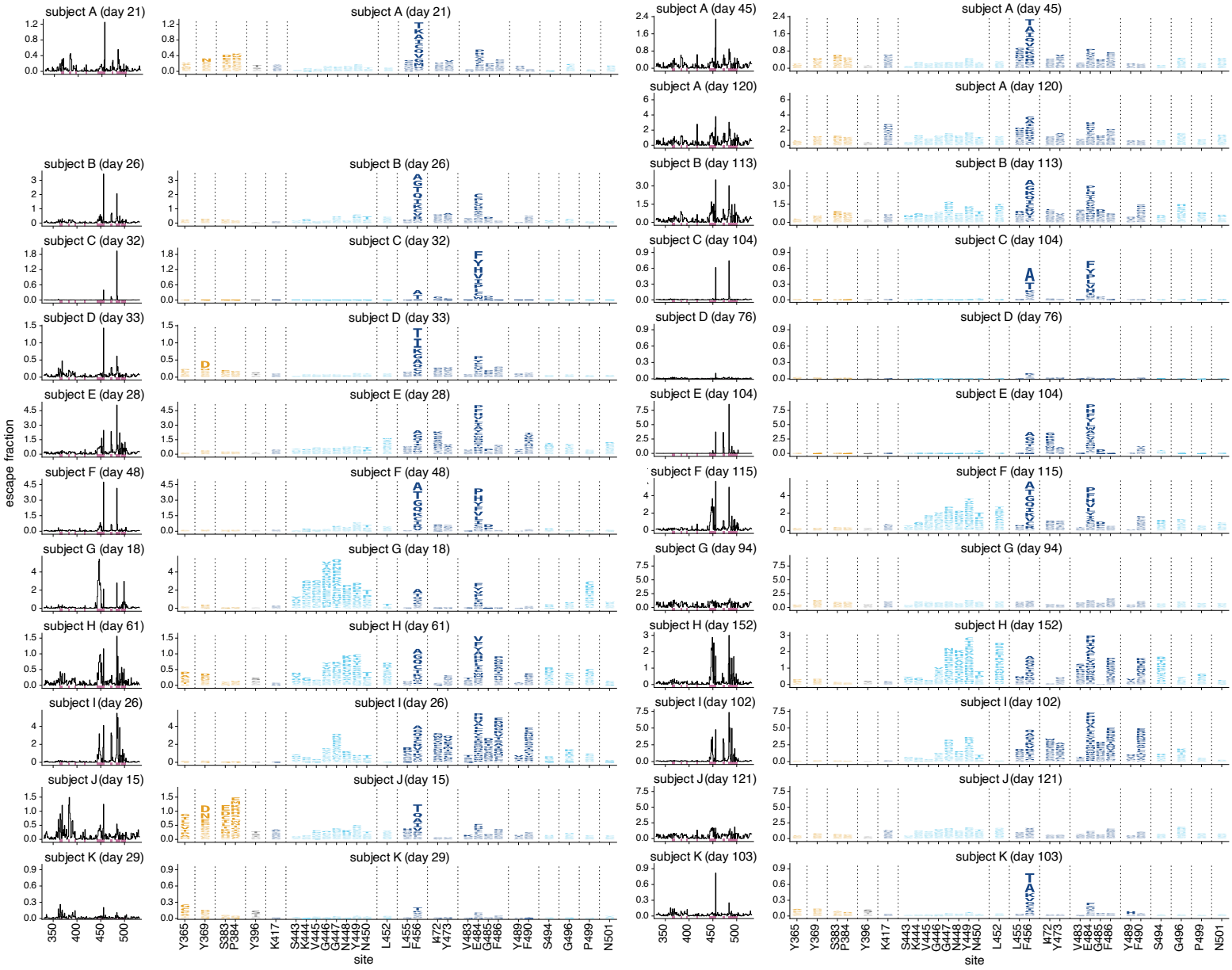

Figure S3. Escape maps over time for all study subjects and time points, related to Figure 4. Escape maps for all individuals and time points, with 2 time points shown side-by-side, ordered as in **Figure 2A**. Escape fractions are comparable across sites within a sample, but not necessarily between samples due to the use of sample-specific FACS gates—therefore, for each sample, the y-axis is scaled independently (see **Methods**). Sites are colored by RBD epitope region as in **Figure 2**. Sites shown in logo plots, highlighted in purple in line plots at left, are sites of strong escape for any of the 23 plasma, plus sites K417 and N501. Interactive versions of these escape maps are available at https://jbloomlab.github.io/SARS-CoV-2-RBD_MAP_HAARVI_sera/.

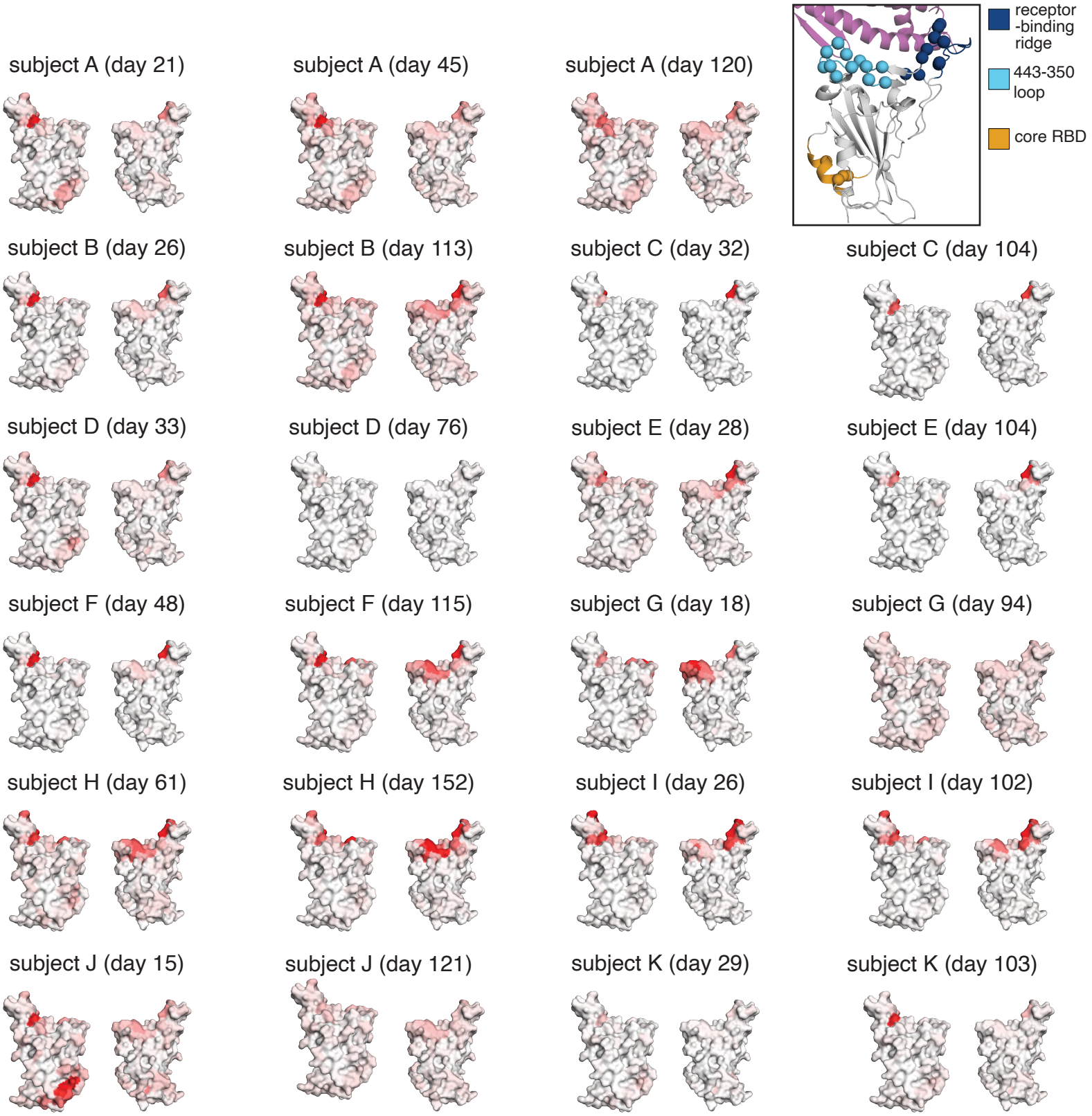

Figure S4. Regions in the RBD where mutations reduce binding by plasma antibodies for all study subjects and samples over time, related to Figure 4. The structures show the effects of mutations at each site projected onto the RBD structure using a white-to-red color scale as in **Figure 3A-D**. The color scale for each plasma is scaled to span the same range as the y-axis for that plasma in **Figure S3**. Top right inset: the alpha-carbon of any site of strong escape (all sites shown in the logo plots in **Figure S3**) is shown as a sphere on a cartoon representation of the RBD (PDB 6M0J). The RBD is colored as in **Figure 2B**. Interactive versions of these structural visualizations are available at https://jbloomlab.github.io/SARS-CoV-2-RBD_MAP_HAARVI_sera/.

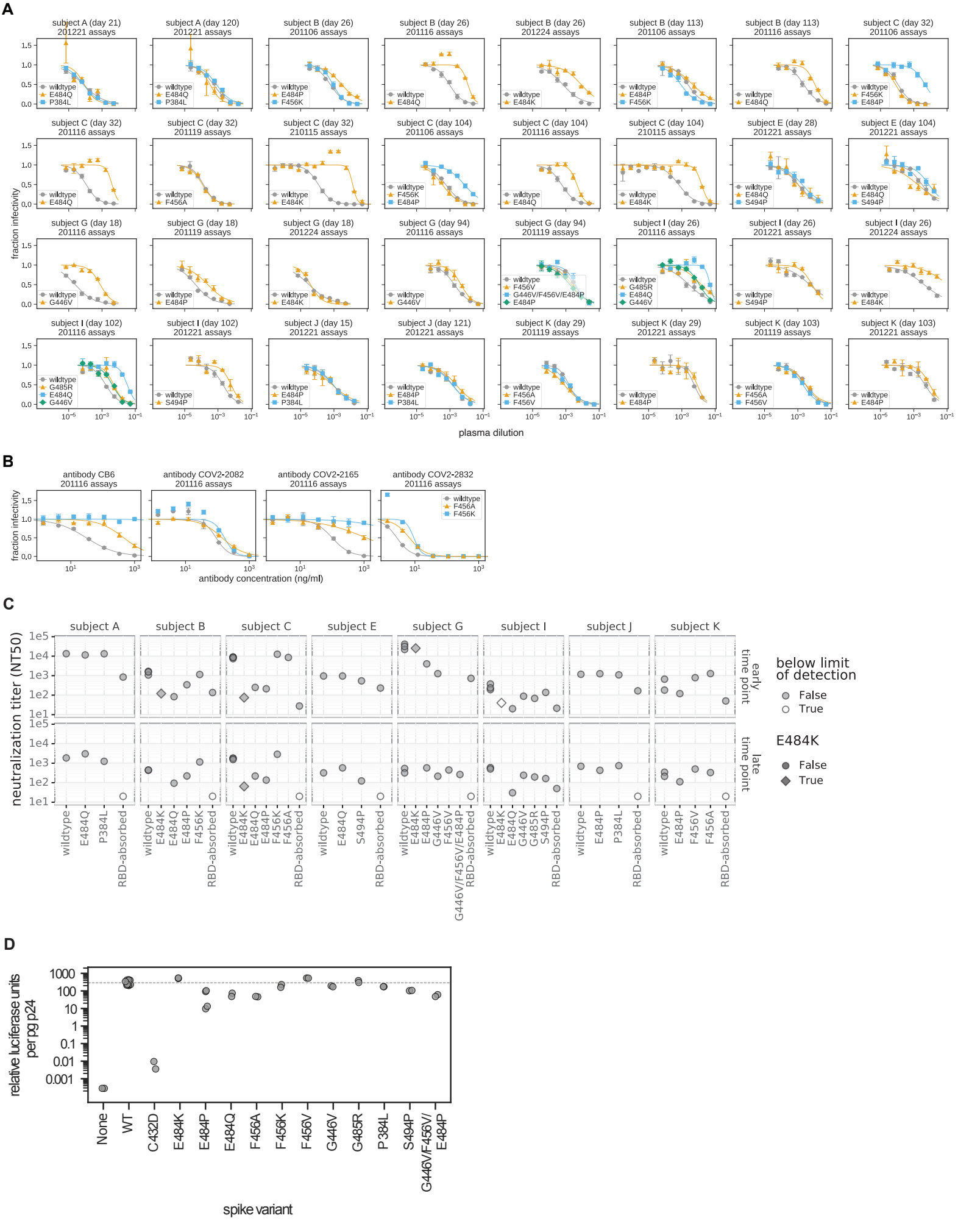
A
subject A (day 21) 201221 assays
wildtype E484Q P384L
subject A (day 120) 201221 assays
wildtype E484Q P384L
subject B (day 26) 201106 assays
wildtype E484P F456K
subject B (day 26) 201116 assays
wildtype E484Q
subject B (day 26) 201224 assays
wildtype E484K
subject B (day 113) 201106 assays
wildtype E484P F456K
subject B (day 113) 201116 assays
wildtype E484Q
subject C (day 32) 201106 assays
wildtype F456K E484P
subject C (day 32) 201116 assays
wildtype E484Q
subject C (day 32) 201119 assays
wildtype F456A
subject C (day 32) 210115 assays
wildtype E484K
subject C (day 104) 201106 assays
wildtype F456K E484P
subject C (day 104) 201116 assays
wildtype E484Q
subject C (day 104) 210115 assays
wildtype E484K
subject E (day 28) 201221 assays
wildtype E484Q S494P
subject E (day 104) 201221 assays
wildtype E484Q S494P
subject G (day 18) 201116 assays
wildtype G446V
subject G (day 18) 201119 assays
wildtype E484P
subject G (day 18) 201224 assays
wildtype E484K
subject G (day 94) 201116 assays
wildtype G446V
subject G (day 94) 201119 assays
wildtype F456V G446V/F456V/E484P E484P
subject I (day 26) 201116 assays
wildtype G485R E484Q G446V
subject I (day 26) 201221 assays
wildtype S494P
subject I (day 26) 201224 assays
wildtype E484K
subject I (day 102) 201116 assays
wildtype G485R E484Q G446V
subject I (day 102) 201221 assays
wildtype S494P
subject J (day 15) 201221 assays
wildtype E484P P384L
subject J (day 121) 201221 assays
wildtype E484P P384L
subject K (day 29) 201119 assays
wildtype F456A F456V
subject K (day 29) 201221 assays
wildtype E484P
subject K (day 103) 201119 assays
wildtype F456A F456V
subject K (day 103) 201221 assays
wildtype E484P
fraction infectivity
plasma dilution
B
antibody CB6 201116 assays
antibody COV2-2082 201116 assays
antibody COV2-2165 201116 assays
antibody COV2-2832 201116 assays
wildtype F456A F456K
fraction infectivity
antibody concentration (ng/ml)
C
subject A
subject B
subject C
subject E
subject G
subject I
subject J
subject K
neutralization titer (NT50)
early time point
late time point
below limit of detection
False
True
E484K
False
True
wildtype E484Q P384L RBD-absorbed
wildtype E484K E484Q E484P F456K RBD-absorbed
wildtype E484K E484Q E484P F456K F456A RBD-absorbed
wildtype E484Q S494P RBD-absorbed
wildtype E484K E484P G446V F456V G446V/F456V/E484P RBD-absorbed
wildtype E484K E484Q G446V G485R S494P RBD-absorbed
wildtype E484P P384L RBD-absorbed
wildtype E484P F456V F456A RBD-absorbed
D
relative luciferase units per pg p24
None WT C432D E484K E484P E484Q F456A F456K F456V G446V G485R P384L S494P G446V/F456V/E484P
spike variant

Figure S5. Full curves for all assays testing how RBD mutations affected viral neutralization, related to Figure 5. (A) The x-axis gives the plasma dilution, and the y-axis gives the fraction of viral infectivity remaining at that dilution. A different plot facet is shown for each plasma (labeled by subject and day of collection) and assay date. The neutralization curves were fit and plotted using `neutcurve` (https://jbloomlab.github.io/neutcurve/, version 0.5.1) and fitting 2-parameter Hill curves with the baselines fixed at one and zero to calculate IC50s. These IC50s were then used to determine the fold-change values plotted in **Figure 5A-C**, comparing each mutant to the wildtype run on the same assay date. Note that NT50 is the reciprocal of the IC50. The curves plotted in **Figure 5D** recapitulate data plotted in this panel, but aggregate mutants across several assay dates and show the wildtype curve for just the first assays date. This aggregation across assay dates is well supported since the wildtype was re-run on each assay date and always yielded very similar IC50s for any given plasma. **(B)** Neutralization curves for monoclonal antibodies run against mutations to F456. Our previous escape mapping showed that F456A/K mutations escape binding by the anti-SARS-CoV-2 RBD monoclonal antibodies COV2-2165 and CB6 (also known as LY-CoV016), but not by COV2-2082 or COV2-2832 (Greaney et al., 2020; Shi et al., 2020; Starr et al., 2021; Zost et al., 2020a). The neutralization assays shown here supported this mapping, and demonstrated that mutations at F456 can indeed greatly reduce neutralization by monoclonal antibodies. **(C)** Absolute neutralization titer (NT50) for each tested plasma and RBD mutant. The numerical IC50s from all curves in both panels are available at https://github.com/jbloomlab/SARS-CoV-2-RBD_MAP_HAARVI_sera/blob/main/experimental_validations/results/mutant_neuts_results/mutants_foldchange_ic50.csv. **(D)** Viral entry titers for key RBD mutants. Titers were measured as relative luciferase units (RLU) normalized to p24 (in picograms) measured by ELISA. The median wildtype titer was 291 RLU/pg p24 or 3.82e8 RLU/mL, and is shown with a dotted horizontal line. "None" is virus-like particles with no spike protein, and C432D disrupts a critical disulfide bond and RBD folding (Starr et al., 2020).